

Preparation and Enhanced Electrochemical Anode Performance of Si/Graphene Nanocomposites

Dongfang Wang,¹ Fulin Li,² Guangxing Ping,¹ Da Chen,^{1,*} Meiqiang Fan,¹ Laishun Qin,¹ Liqun Bai,³ Guanglei Tian,¹ Chunju Lu,¹ Kangying Shu¹

¹ College of Materials Science & Engineering, China Jiliang University, Hangzhou, Zhejiang province 310018, China

² Zhejiang Tianneng Energy Technology Co., Ltd., Zhicheng Industry Zone, Changxing County, Zhejiang Province 313100, China

³ School of Sciences, Zhejiang Agriculture and Forestry University, Hangzhou 311300, Zhejiang Province, China

*E-mail: dchen_80@hotmail.com

Received: 13 May 2013 / Accepted: 18 June 2013 / Published: 1 July 2013

Si/graphene nanocomposites with different weight ratios were successfully prepared by ball-milling of commercially available Si nanoparticles and graphene oxide (GO) nanosheets. It was demonstrated that Si nanoparticles within the Si/graphene nanocomposites were well distributed onto the flexible graphene nanosheets. Compared to the pristine Si nanoparticles anode, the Si/graphene composite anodes showed an enhanced reversible capacity and cyclic performance, highlighting the advantages of anchoring Si nanoparticles on graphene sheets. The enhancement on electrochemical performance could be ascribed to the fact that graphene nanosheets within the Si/graphene nanocomposites could act as a flexible conductive scaffold network to maintain excellent electronic contact, improve ionic conductivity and charge transfer as well as accommodate the large volume change of Si during the lithiation/delithiation process.

Keywords: Silicon/graphene nanocomposites; Anode materials; Lithium ion batteries; Cycling performance

1. INTRODUCTION

Rechargeable lithium-ion batteries (LIBs) are currently the predominant power sources for various commodities, ranging from portable electronics to electric vehicles (EVs), and also in large-scale energy storage. Tremendous attention has been paid to this electrochemical device due to its advantages such as safety, low cost, and high energy density. The increasing demand for advanced LIBs with more excellent performance, however, has driven intense research on high-capacity anode

or cathode materials. With respect to the anode materials, silicon has been considered as one of the most promising candidate for LIBs due to its highest known theoretical charge capacity (4200 mAh g^{-1}), which is ten times higher than that of commercial graphite anode (372 mAh g^{-1}). The ultrahigh capacity of silicon stems from the fact that it exhibits electrochemical alloying storage behavior, corresponding to the fully lithiated composition of $\text{Li}_{4.4}\text{Si}$, unlike the insertion mechanism of graphite [1].

However, before the full utilization of Si as a practical anode material, there are still two major challenges. It is well known that a gigantic volume expansion ($>300\%$) and the high mechanical stresses accompany the lithium alloying process with Si to form $\text{Li}_{4.4}\text{Si}$ during cycling. As a result, silicon would pulverize, thus leading to electrical disconnection from the current collector, and eventual capacity fading [2]. Another practical limitation to the high performance of silicon comes from its poor semiconductive charge transportation (only about $10^{-5} \text{ S cm}^{-1}$, compared with 10^3 S cm^{-1} of graphite) that hinders the electrode redox process and electronic diffusion [3].

In order to overcome the aforementioned demerits, many approaches have been reported on accommodating the swing in volume and/or accelerating charge transfer within the electrode, including the development of novel Si nanostructures (such as nanowires [4], thin-films with nanoparticles [5, 6]), the fabrication of the core-shell structure [7, 8], the addition of different conductive materials [9] and the formation of Si/C composites [10]. Among these approaches, it is believed that carbon-based materials, as an appropriate alternative, can buffer the volume changes and also improve the electronic and ionic conductivities [11]. On the other hand, graphene, a monolayer of carbon material with carbon atoms arranged into a honeycomb structure, exhibits novel properties, especially the excellent electrical conductivity, large surface area, chemical stability and high mechanical flexibility [12,13]. These properties make it an excellent active matrix for the preparation of Si/graphene nanocomposites to improve the electrochemical performance of Si-based materials. The enhanced electrochemical performance can be attributed to the fact that graphene can serve as a strong scaffold network to help accommodate the volume change of the Si nanoparticles during charging/discharging and ensure facile electron transport [14].

In this work, Si/graphene nanocomposites have been prepared by using high energy ball-milling followed by thermal treatment, and their electrochemical performances as anode materials have been also investigated. The research objective of the present work is to develop the Si/graphene nanocomposites as an alternative anode for high performance LIBs.

2. EXPERIMENTAL

2.1 Preparation of Si/graphene nanocomposites

Graphene oxide (GO) was produced from natural graphite powder by a modified Hummers' method as reported elsewhere [15,16]. The Si/graphene nanocomposites were synthesized by ball-milling of Si nanoparticles and GO nanosheets. Typically, the mixture of commercially available nanosize Si (80 nm, Alfa Aesa) and GO were blended in an 8 wt% *N*-methyl-2-pyrrolidone (NMP)

solution of poly (vinylidene fluoride) (PVDF). The obtained mixture was then milled for 20 h with agate balls as the mixing media at a rotary rate of 350 r/min, and finally vacuum-dried at 100 °C for 6 h. (It should be noted that the ball-milling time is very important for the quality of Si/graphene nanocomposites. In our case, it was found that the obvious aggregates of GO nanosheets still existed in the mixture of Si nanoparticles, GO and PVDF/NMP if the ball-milling time was less than 12 h. However, the mixture became homogeneous when the ball-milling time was improved to 20 h.) To reduce GO and carbonize PVDF, the dried composite was further calcined at 700 °C in an H₂ (5 vol%)/N₂ (95 vol%)-flowing tube furnace for 3 h with a heating ramp of 5 °C min⁻¹. This kind of graphene/nanosized Si nanocomposite was labeled as SiG1 and SiG2, with the weight ratios of Si particles to GO as 80:20 and 60:40, respectively.

2.2 Characterizations

The morphologies of the samples were characterized by using the field-emission scanning electron microscope (FESEM, JEOL JSM-6700F, Japan). The crystal phase identification of samples was performed on a X-ray diffraction (XRD) (Bruker Axs D2 PHASER, Germany) with Cu K α radiation ($\lambda = 0.15406\text{nm}$). The 2θ range used in the measurements was from 10° to 80° at room temperature. Thermogravimetric analysis (TGA) was carried out using a thermogravimetric analyzer (Mettler, SMP/PF7548/MET/600W, Switzerland) with a heating rate of 10 °C min⁻¹ in air. The Fourier transform infrared (FTIR) absorption spectrum was obtained by FTIR spectrophotometer (Bruker Tensor 27, Germany). The Raman spectra were determined by a Raman spectroscopy (RENISHAW WIRE3.3 confocal with 532 nm diode laser excitation).

2.3 Electrochemical measurement

Electrochemical properties of the products were measured using coin cells. The working electrodes were prepared by casting the slurry consisting of 80 wt% of active material (commercial Si nanoparticles or as-prepared Si/graphene nanocomposites), 10 wt% of conductive Super P carbon black, and 10 wt% of PVDF (Alfa Aesar) onto a copper foil. The electrolyte consisted of a solution of 1 M LiPF₆ in ethylene carbonate (EC)/diethyl carbonate (DEC) (1:1 v/v). Lithium foil was used as counter electrodes. These cells were assembled in an argon-filled glovebox (MIKROUNA) and galvanostatically cycled between 0.01 V and 1.5 V (vs. Li/Li⁺) on a multi-channel battery cycler (Land Battery Test System). The ac impedance was measured at an Autolab electrochemical workstation (CH Instruments), with the frequency range and voltage amplitude set as 100 kHz to 0.01 Hz and 10 mV, respectively.

3. RESULTS AND DISCUSSION

3.1 Characterizations of Si/graphene nanocomposites

Figure 1 shows the FESEM images of the commercial Si nanoparticles and the as-prepared Si/graphene nanocomposites. As shown in Figure 1a, the commercial Si nanoparticles were spherical-

shaped particles with the size of about 50~100 nm, which were prone to get aggregated. As for the as-prepared Si/graphene nanocomposites (Figure 1b and c), the graphene sheets and Si nanoparticles were distinguished clearly, and the Si nanoparticles with the size of about 50~100 nm were well separated from each other and tightly bonded to the transparent graphene sheets.

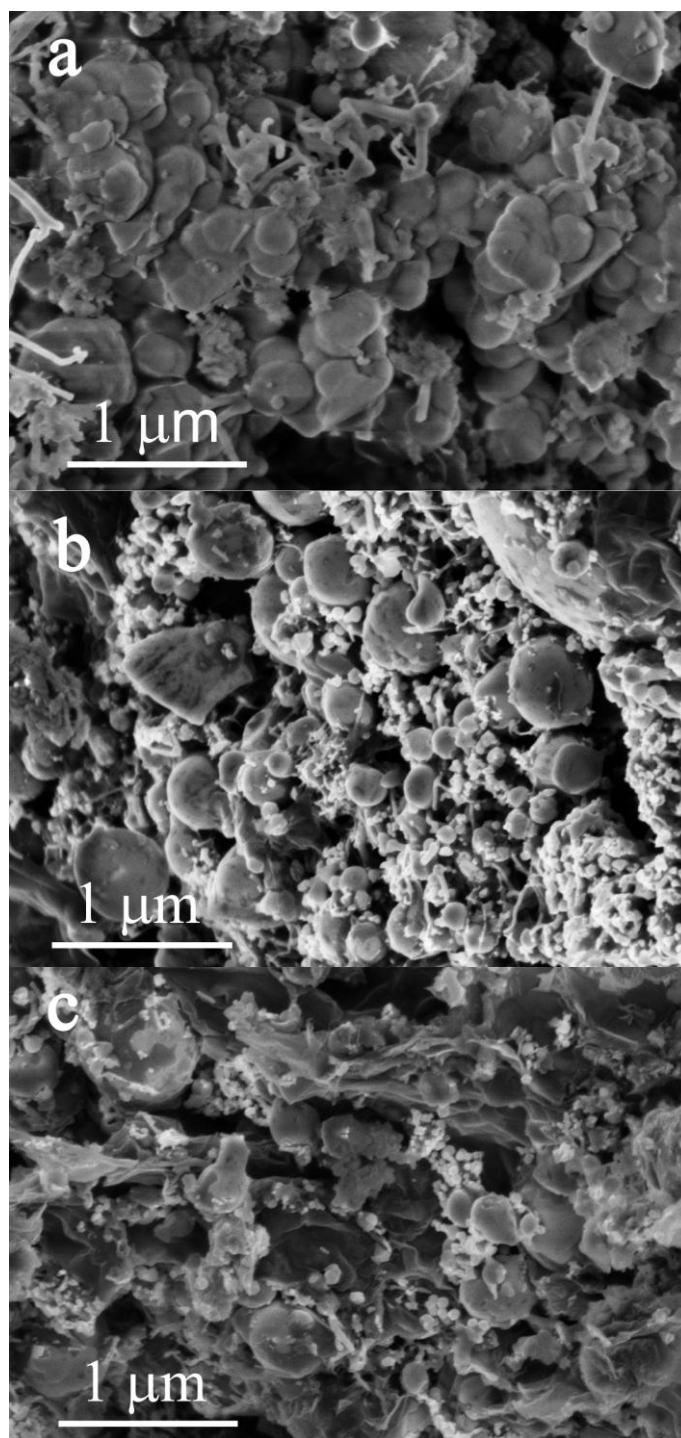


Figure 1. FESEM images of (a) pure Si nanoparticles, (b) SiG1 (Si/graphene nanocomposites with the weight ratio of Si to GO as 80:20) and (c) SiG2 (Si/graphene nanocomposites with the weight ratio of Si to GO as 60:40).

This indicates that the high-energy ball milling process could prevent Si nanoparticles from agglomeration and enable a firm attachment of these nanoparticles to the graphene support. Moreover, compared to the SiG1 nanocomposite, the higher content of graphene sheets in the SiG2 nanocomposite was favorable to form more uniform composite, by restricting more Si particles in the graphene matrix or linking more particles on the larger surface of graphene.

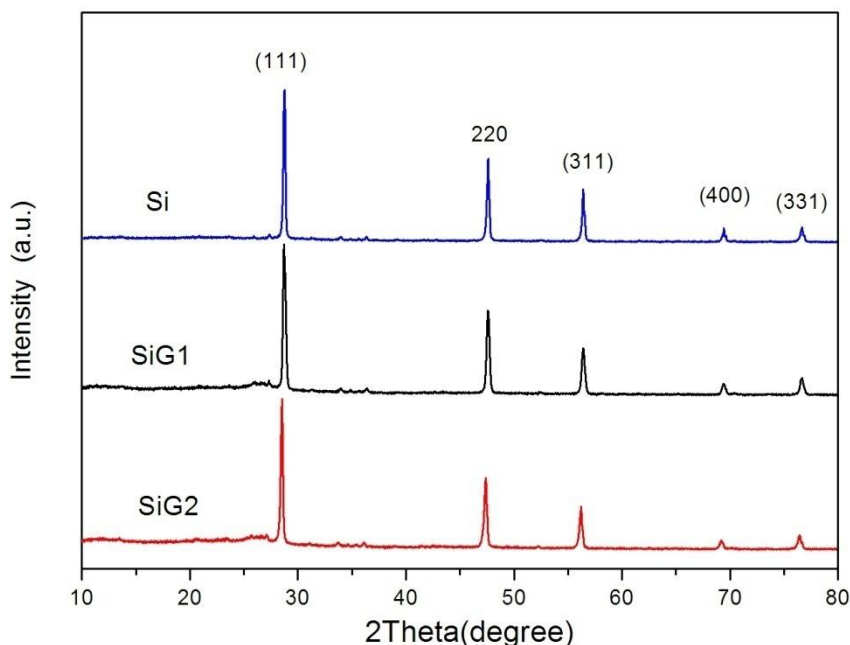


Figure 2. XRD patterns of pure Si nanoparticles, SiG1 and SiG2 nanocomposites.

The XRD patterns obtained from the as-prepared SiG1 and SiG2 nanocomposites together with the commercial Si nanoparticles were shown in Figure 2. For the bare Si nanoparticles, all the peaks could be well assigned to the pure phase of well-crystallized Si with cubic structure (JCPDS No. 77-2107). In addition, Si/graphene nanocomposites (SiG1 and SiG2) showed similar XRD patterns to that of Si nanoparticles, except that there appeared a diffraction peak at $2\theta = 26.0^\circ$, which could be attributed to the graphite-like (002) structure from graphene [17]. This indicates that GO was reduced to graphene during the calcination process. Furthermore, the broad character of the peak at 26.0° also proves that graphene was homogeneously distributed in the nanocomposites without stacking or agglomeration [18].

The structure of Si/graphene nanocomposites was further investigated by FTIR spectra. As shown in Figure 3, the most characteristic features of GO include the broad, intense band of O-H stretching vibration at $3000\sim 3700\text{ cm}^{-1}$, as well as the bands of C=O, C-OH and C-O stretching vibration at 1634 cm^{-1} , 1401 cm^{-1} and 1114 cm^{-1} , respectively [19]. This indicates that GO could contain small amount of H_2O and many oxygen functional groups (such as hydroxyl, carbonyl, carboxylic and epoxy) on its surface. For the spectra of Si nanoparticles and Si/graphene nanocomposites (SiG1 and SiG2), the strongly absorption at about 1100 cm^{-1} was attributed to the anti-

symmetrical vibration of Si-O-Si [20, 21]. Besides, compared to those in GO, the intensities of the bands corresponding to the oxygen functional groups and O-H stretching vibration in SiG1 and SiG2 obviously decreased, suggesting the effective reduction of GO sheets by thermal treatment.

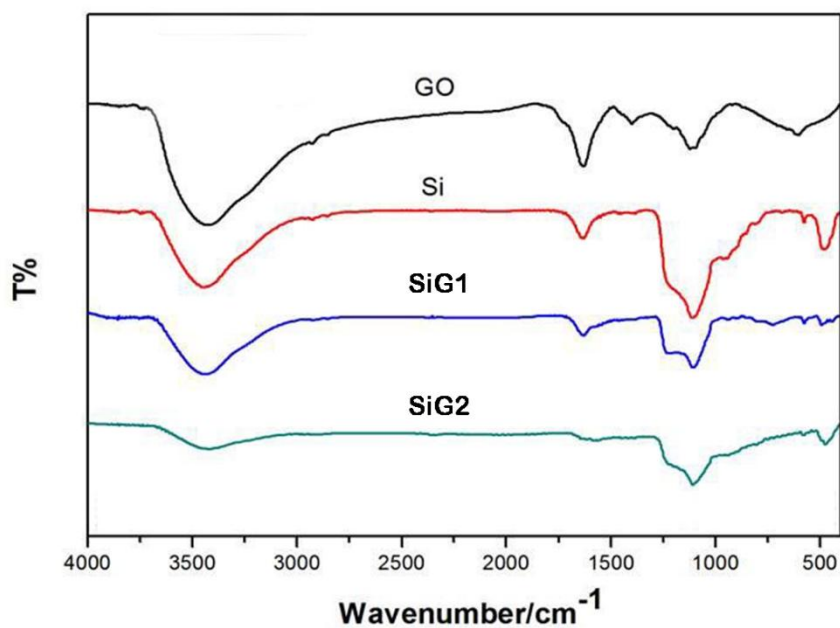


Figure 3. FT-IR spectra of pure Si nanoparticles, SiG1 and SiG2 nanocomposites.

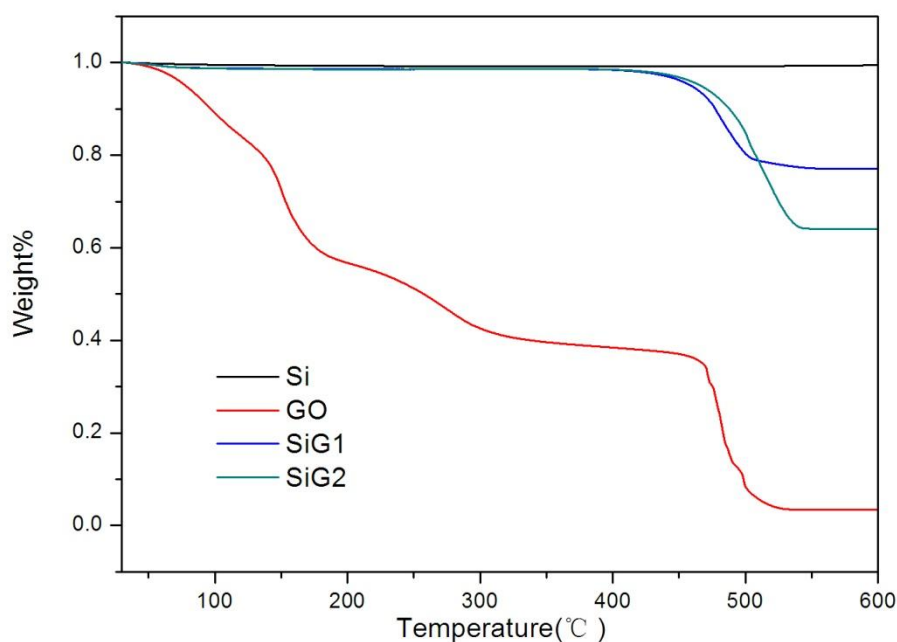


Figure 4. TGA curves of Si nanoparticles, GO, SiG1 and SiG2 nanocomposites in air.

To determine the content of Si in the Si/graphene composites, TG/DSC measurements were performed in air from room temperature to 600 °C, as shown in Figure 4. For the GO curve, the weight loss under 300 °C could be ascribed to the loss of adsorbed water and pyrolysis of the labile oxygen-containing functional groups, and the weight loss occurred at 300~500 °C due to the complete oxidation reaction of GO. For Si nanoparticles, however, the weight increased a little bit from room temperature to 600 °C due to the formation of negligible SiO_x, indicating that the oxidation of Si powder in air was not significant at 600 °C. Thus, it is reasonable to determine the content of graphene in the nanocomposites from the largest weight loss at 300~500 °C in the TGA curve of Si/graphene nanocomposites. It can be estimated that the largest weight loss in the SiG1 and SiG2 nanocomposites was approximately 21.5 wt% and 34 wt% at 300~500 °C, respectively. Therefore, the Si content in the SiG1 and SiG2 nanocomposites was calculated to be 78.5 wt% and 66 wt%, respectively, which was on the whole consistent with the feed ratio of Si (80 wt% and 40 wt%) during the ball milling process.

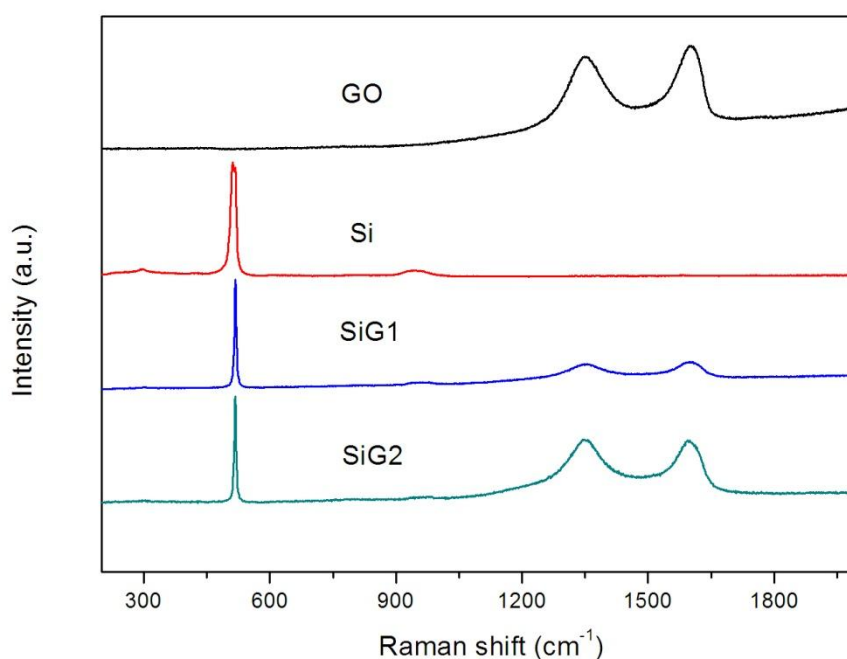


Figure 5. Raman spectra for Si nanoparticles, GO, SiG1 and SiG2 nanocomposites

Figure 5 shows the Raman spectra of Si/graphene nanocomposites (SiG1 and SiG2), along with the bare Si nanoparticles and GO sheets. As shown, the bare Si nanoparticles exhibited a characteristic sharp peak at 511 cm⁻¹, which was assigned to Si [22]. For SiG1, the main peak at about 517 cm⁻¹ was in agreement with the data in the spectrum of Si nanoparticles, and another two peaks at around 1355 cm⁻¹ and 1590 cm⁻¹ were identified respectively as the D band and G band of graphene [23]. The Raman spectrum of SiG2 was similar to that of SiG1, except that the intensities of the two peaks assigned to graphene were much stronger due to the higher content of graphene sheets. In addition, compared to GO, the I_D/I_G intensity ratios of Si/graphene nanocomposites (SiG1 and SiG2) were

slightly decreased after thermal reduction. This decrease could be attributed to the increase of the size of the in-plane sp^2 domain [24].

3.2 Electrochemical measurements

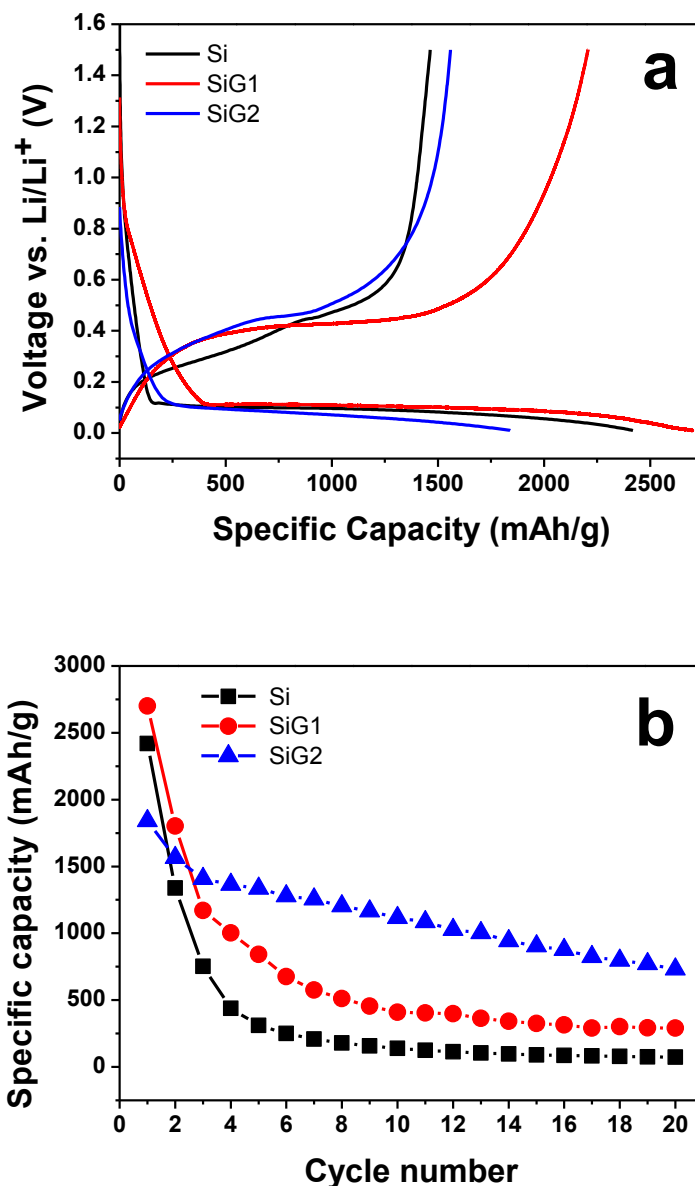


Figure 6. (a) The charge–discharge voltage profiles of the cells with SiG1 and SiG2 composite anodes compared with the Si anode for the first cycle. The current density was 400 mA/g. (b) Cycling performance of Si anode, SiG1 and SiG2 composite anodes. The current density was 400 mA/g.

In order to explore the electrochemical performance of these materials, as-prepared Si/graphene nanocomposites were used as LIB anodes for electrochemical evaluation. Figure 6a shows the charge-discharge voltage profiles of the cells with SiG1 and SiG2 composite anodes compared with the Si

anode for the first cycle. The initial charge and discharge capacities were 1464 mAh/g and 2420 mAh/g for the Si nanoparticles anode, respectively, with an initial Coulombic efficiency of 60.5%. The irreversible capacity ratio of 39.5% could be assigned to the decomposition of electrolyte, forming a solid/electrolyte interphase (SEI) on the electrode surface [25], and to the irreversible insertion of Li ions into silicon particles. In contrast, the SiG1 composite anode displayed a capacity of 2700 and 2207 mAh g⁻¹ for the first discharge and charge processes, respectively. Compared with Si nanoparticles (60.5%), the initial coulombic efficiency of the SiG1 composite anode was improved to 81.7%. Furthermore, with the increase of the graphene content, the SiG2 composite anode showed a higher initial coulombic efficiency (84.8%), though it delivered an initial discharge capacity of only about 1840 mAh/g due to the lower Si content in the nanocomposite. Thus, it can be seen that the reversible capacity retention and initial coulombic efficiency of the Si/graphene nanocomposites represented a significant improvement over those of Si nanoparticles.

Figure 6b shows the discharge-charge cycling performances of Si and Si/graphene anodes for the first fifty cycles at the current density of 400 mA g⁻¹. In the case of Si nanoparticles anode, the 1st cycle discharge capacity had a relatively high value of 2420 mAh g⁻¹. However, the Si anodes displayed poor cycling performance which showed severe decay just after several cycles. It was found that the discharge capacity retention for the Si nanoparticles anode was only 12.8% and 1.8% after 5 cycles and 50 cycles, respectively.

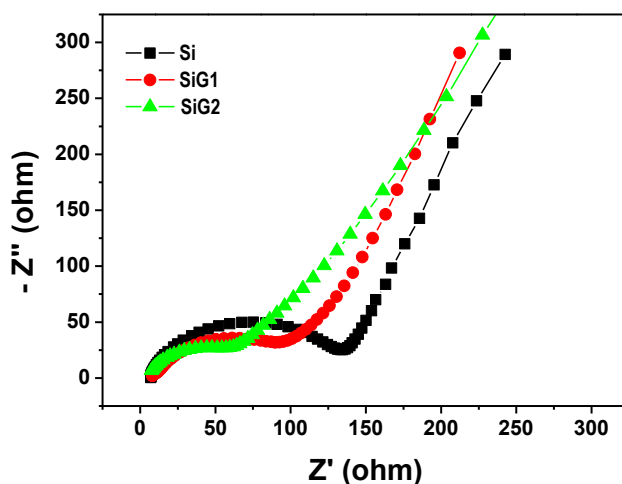


Figure 7. Nyquist plots of Si nanoparticles, SiG1 and SiG2 nanocomposites-based anodes at a discharged potential of 0.1 V (vs. Li/Li⁺) from 100 kHz to 10 mHz.

In comparison, the Si/graphene nanocomposites significantly improved the anode stability for both samples of SiG1 and SiG2. After fifty cycles, the SiG1 and SiG2 composite anodes had the discharge capacity of 304 mAh g⁻¹ (~11.3% of the initial capacity) and 681 mAh g⁻¹ (~37.0% of the initial capacity), respectively. These results clearly show that the anchoring of graphene with Si nanoparticles played an important role in improving the electrochemical performance. The high reversible capacity and improved cycle stability could be attributed to the porosity between the graphene sheets that was favorable for Li ion transport, the interleaved electron transfer highways built

up from high conductive graphenes, and the flexible graphenes that played a “flexible confinement” function to enwrap Si nanoparticles for inhibiting the volume change, alleviating the stress of Si nanoparticles, and preventing the detachment and agglomeration of pulverized Si nanoparticles during cycling [11, 18].

Figure 7 shows the Nyquist plots of the Si nanoparticles anode, the SiG1 and SiG2 composite anodes at a discharged potential of 0.1 V vs. Li/Li⁺ after charge–discharge for three cycles, which further demonstrated the favorable electrical connection and charge transport between graphene and Si nanoparticles. The impedance curves show one compressed semicircle in the medium-frequency region, which could be assigned to the charge-transfer resistance (R_{ct}), and an inclined line in the low-frequency range, which could be considered as Warburg impedance [11]. As shown, both the Si/graphene composites anodes (SiG1 and SiG2) exhibited a smaller charge-transfer resistance (R_{ct}) than the Si nanoparticles anode, indicating the enhanced ionic conductivity and faster charge transfer of the Si/graphene nanocomposites. Also, compared with the SiG1 composite anode, the SiG2 composite anode showed a decreased charge-transfer resistance due to the increase of the graphene content in the Si/graphene nanocomposites. The enhancement of Si/graphene nanocomposites in ionic conductivity and charge transfer could be ascribed to the high conductivity of graphene as well as the high surface area and porous structure of the graphene, which could facilitate the penetration of the electrolyte. The difference of the charge-transfer resistance was another reasonable explanation for the enhancement of electrochemical cycle performance of the Si/graphene nanocomposites anode.

4. CONCLUSIONS

In summary, Si/graphene nanocomposites for LIBs anode materials were successfully prepared using high-energy ball-milling followed by thermal treatment process. Experimental results demonstrated that for the Si/graphene nanocomposites, the Si nanoparticles with the size of about 50–100 nm were well distributed onto the flexible graphene nanosheets. Compared to the pristine Si anode, the Si/graphene composite anodes showed an enhanced reversible capacity and cyclic performance, highlighting the advantages of anchoring Si nanoparticles on graphene sheets. The significant enhancement on electrochemical performance could be ascribed to the fact that the graphene nanosheets within the Si/graphene nanocomposites could not only alleviate the aggregation of Si nanoparticles and accommodate large volume changes of Si nanoparticles, but also enhance the ionic conductivity and charge transfer during the lithiation/delithiation process.

ACKNOWLEDGMENTS

This work was financially supported by the National Natural Science Foundation of China (21003111, 21003112, 51002147 and 11075147).

References

1. B. A. Boukamp, G. C. Lesh and R. A. Huggins, *J. Electrochem. Soc.*, 128 (1981) 725-729.
2. Y. Yu, L. Gu, C. Zhu, S. Tsukimoto and P. A. van Aken, *J. Mater.*, 22 (2010) 2247-

- 2250.
3. X. L. Wang and W.Q. Han, *ACS Appl. Mater. Interfaces*, 2 (2010) 3709-3713.
 4. V. Chakrapani, F. Rusli, M. A. Filler and P. A. Kohl, *J. Power Sources*, 205 (2012) 433-438.
 5. U. Kasavajjula, C. S. Wang and A. J. Appleby, *J. Power Sources*, 163 (2007) 1003-1039.
 6. J. Lai, H. J. Guo, Z. X. Wang, X. H. Li, X. P. Zhang, F. X. Wu and P. Yue, *J. Alloys Compd.*, 530 (2012) 30-35.
 7. Y. Hwa, W. S. Kim, S. H. Hong and H. J. Sohn, *Electrochim. Acta*, 71 (2012) 201-205.
 8. B. S. Lee, S. B. Son, K. M. Park, J. H. Seo, S. H. Lee, I. S. Choi, K. H. Oh and W. R. Yu, *J. Power Sources*, 206 (2012) 267-273.
 9. A. Gohier, B. Laik, K. H. Kim, J. L. Maurice, J. P. Pereira-Ramos, C. S. Cojocaru and P. T. Van, *Adv. Mater.*, 24 (2012) 2592-2597.
 10. G. X. Wang, J. H. Ahn, J. Yao, S. Bewlay and H. K. Liu, *Electrochem. Commun.*, 6 (2004) 689-692.
 11. S. L. Chou, J. Z. Wang, M. Choucair, H. K. Liu, J. A. Stride and S. X. Dou, *Electrochem. Commun.*, 12 (2010) 303-306.
 12. K. I. Bolotin, K. J. Sikes, Z. Jiang, M. Klima, G. Fudenberg, J. Hone, P. Kim and H. L. Stormer, *Solid State Commun.*, 146 (2008) 351-355.
 13. H. L. Wang, Y. A. Yang, Y. Y. Liang, J. T. Robinson, Y. G. Li, A. Jackson, Y. Cui and H. J. Dai, *Nano Lett.*, 11 (2011) 2644-2647.
 14. X. S. Zhou, Y. X. Yin, A. M. Cao, L. J. Wan and Y. G. Guo, *ACS Appl. Mater. Interfaces*, 4 (2012) 2824-2828.
 15. W. S. Hummers and R. E. Offeman, *J. Am. Chem. Soc.*, 80 (1958) 1339-1339.
 16. Y. X. Xu, H. Bai, G. W. Lu, C. Li and G. Q. Shi, *J. Am. Chem. Soc.*, 130 (2008) 5856-5857.
 17. K. Raidongia, A. Nag, K. P. S. S. Hembram, U. V. Waghmare, R. Datta and C. N. R. Rao, *Chem. Eur. J.*, 16 (2010) 149-157.
 18. H. F. Xiang, K. Zhang, G. Ji, J. Y. Lee, C. Zou, X. D. Chen and J. S. Wu, *Carbon*, 49 (2011) 1787-1796.
 19. J. Shen, M. Shi, H. Ma, B. Yan, N. Li and M. Ye, *Mater. Res. Bull.*, 46 (2011) 2077-2083.
 20. A. Gupta and H. Wiggers, *Physica E*, 41 (2009) 1010-1014.
 21. P. Kale, A. C. Gangal, R. Edla and P. Sharma, *Int. J. Hydrogen Energ.*, 37 (2012) 3741-3747.
 22. S. Y. Chew, Z. P. Guo, J. Z. Wang, J. Chen, P. Munroe, S. H. Ng, L. Zhao and H. K. Liu, *Electrochem. Commun.*, 9 (2007) 941-946.
 23. S. Bong, Y. R. Kim, I. Kim, S. Woo, S. Uhm, J. Lee and H. Kim, *Electrochem. Commun.*, 12 (2010) 129-131.
 24. G. X. Wang, J. Yang, J. Park, X. L. Gou, B. Wang, H. Liu and J. Yao, *J. Phys. Chem. C*, 112 (2008) 8192-8195.
 25. Y. Liu, K. Hanai, J. Yang, N. Imanishi, A. Hirano and Y. Takeda, *Electrochem. Solid-State Lett.*, 7 (2004) A369-A372.